

NEW CLASS OF VERY HIGH ENERGY γ -RAY EMITTER: RADIO-DARK MINI-SHELLS SURROUNDING AGN JETSMOTOKI KINO¹, HIROTAKA ITO², NOZOMU KAWAKATU³, AND MONICA ORIENTI^{4, 5}*Draft version February 4, 2013*

ABSTRACT

We explore non-thermal emission from a shocked interstellar medium, which is identified as an expanding shell, driven by a relativistic jet in active galactic nuclei (AGNs). In this work, we particularly focus on parsec-scale size mini-shells surrounding mini radio lobes. From radio to X-ray band, the mini radio lobe emission dominates the faint emission from the mini-shell. On the other hand, we find that inverse-Compton (IC) emission from the shell can overwhelm the associated lobe emission at very high energy (VHE; $E > 100$ GeV) γ -ray range, because energy densities of synchrotron photons from the lobe and/or soft photons from the AGN nucleus are large and IC scattering effectively works. The predicted IC emission from nearby mini-shells can be detected with the *Cherencov Telescope Array* (CTA) and they are potentially a new class of VHE γ -ray emitters.

Subject headings: active galactic nuclei (AGNs) — galaxies: jets — radio continuum: galaxies

1. INTRODUCTION

Radio-loud active galactic nuclei (AGNs) are among the most powerful objects in the Universe. According to the standard picture of jets in AGNs, the jets are enveloped in a cocoon consisting of shocked jet material and the cocoon is surrounded by shocked interstellar medium. The shocked ambient region (hereafter we refer to as the shell) is identical to the forward shocked region and it is a fundamental ingredient in the whole AGN jet system. In spite of this, physical properties of shells have not been well studied since they are not bright and remain undetected except for thermal X-ray detections of shells surrounding bubbles in Centaurus A (Croston et al. 2009), NGC3801 (Croston et al. 2007), and in the Galactic center (Su et al. 2010 and reference therein). In radio band, shells are dim (Carilli et al. 1988) and their overall emissions are overwhelmed by the radio bubbles (radio lobes) identical to a portion of the cocoon.

Recently, we indicate a possibility of VHE γ -ray emissions from AGN shells in Ito et al. (2011) (hereafter I11). In I11, the non-thermal emission of a shell is mainly produced by Inverse-Compton (IC) mechanism for compact sources (less than ~ 10 kpc), while synchrotron radiation is more important for larger shells. Physical properties of nearby shells can be proved by the detection of IC emissions using modern Cherenkov telescopes. The examined shell size in I11 was, however, limited to 1 – 100 kpc. In this paper, we complement the work of I11 by exploring smaller shells. I11 indicates that smaller shells may be a new class of VHE γ -ray emitter in the universe and in the present work we quantitatively examine the theoretically predicted photon spectra from the mini-shells. To

clarify the detection feasibility by the next generation instrument *Cherencov Telescope Array* (CTA), we further examine the non-thermal emission on 10 pc scale, which corresponds to the smallest scale of radio bubbles ever observed, properly taking into account the $\gamma\gamma$ absorption by extragalactic background light (EBL). The CTA will consist of two arrays of Cherenkov telescopes, which aim to: (a) increase sensitivity by one order of magnitude for deep observations around 1 TeV, (b) boost significantly the detection area and hence detection rates, (c) increase the angular resolution and hence the ability to resolve the morphology of extended sources, (d) provide uniform energy coverage for photons from some tens of GeV to beyond 100 TeV, and (e) enhance the sky survey capability, monitoring capability and flexibility of operation (e.g., Actis et al. 2011; Funk et al. 2012).

In this work, we particularly focus on the nearby mini radio lobes of CORALZs (COmpact RADIO sources at Low-Redshift) which are located at the redshift of $0.005 \leq z \leq 0.16$ (Snellen et al. 2004; de Vries et al. 2009) and less luminous mini lobes which would be detected by deep sensitivity observations in the future by using the next generation radio telescope *Square Kilometer Array* (SKA) with its collecting area distributed over a large geographical area (Lazio 2011 for details of its specification).

2. MODEL

First, we briefly review the model following our previous work I11. For simplicity, we neglect the elongation of cocoon and shell and we adopt the expanding spherical bubble model (see Fig. 1). The shell width at the bubble radius $R(t)$ at the time (t) is denoted as $\delta R(t)$. The mass density of the ambient matter at $R(t)$ is defined as $\rho_a(R(t)) = \rho_0(R(t)/R_0)^{-\alpha}$ ($0 \leq \alpha \leq 2$) where R_0 is the reference radius, $\delta R(t)$ satisfies the relation $\delta R(t) = (\gamma_a - 1)R(t)/[(\gamma_a + 1)(3 - \alpha)]$ where γ_a is the specific heat ratio of the ambient matter (e.g., I11). The thin shell condition $\delta R(t) \ll R(t)$ holds when the expansion velocity has a high Mach number. We further assume that the kinetic power of jet, L_j , is constant in time. The jet kinetic energy is dissipated and deposit-

Electronic address: kino@vsop.isas.jaxa.jp

¹ ISAS/JAXA, 3-1-1 Yoshinodai, 229-8510 Sagami-hara, Japan² Yukawa Institute for Theoretical Physics, Kyoto University, Oiwake-cho Kitashirakawa Sakyo-ku, Kyoto, 606-8502, Japan³ Graduate School of Pure and Applied Sciences, University of Tsukuba, 1-1-1 Tennodai, Tsukuba 305-8571, Japan⁴ Dipartimento di Astronomia, Università di Bologna, via Ranzani 1, I-40127, Bologna Italy⁵ INAF - Istituto di Radioastronomia, via Gobetti 101, 40129 Bologna, Italy

ted as the internal energy of the cocoon and shell. The internal energy drives the cocoon expansion. Note that specifying a fraction of electrons/protons in the jet is irrelevant to the expansion dynamics. Solving the set of equations for the momentum and energy equations for the expanding bubble, $R(t)$ can be expressed as

$$R(t) = C R_0^{\alpha/(\alpha-5)} \left(\frac{L_j}{\rho_0} \right)^{1/(5-\alpha)} t^{3/(5-\alpha)}, \quad (1)$$

where the coefficient C is given by $C = \left[\frac{(3-\alpha)(5-\alpha)^3(\hat{\gamma}_c-1)}{4\pi\{2\alpha^2+(1-18\hat{\gamma}_c)\alpha+63\hat{\gamma}_c-28\}} \right]^{1/(5-\alpha)}$ where $\hat{\gamma}_c$ is the adiabatic index of the cocoon. This is identical to the well known stellar wind model (e.g., Castor et al. 1975; Ostriker and McKee 1988). For convenience, we define the total internal energy deposited in the shell and cocoon as follows: $E_{\text{shell}} = f_{\text{shell}} L_j t$, and $E_{\text{cocoon}} = f_{\text{cocoon}} L_j t$ where the factors f_{shell} and f_{cocoon} can be given by $f_{\text{shell}} = \frac{18(\hat{\gamma}_c-1)(5-\alpha)}{(\hat{\gamma}_a+1)^2[2\alpha^2+(1-18\hat{\gamma}_c)\alpha+63\hat{\gamma}_c-28]}$ and $f_{\text{cocoon}} = (5-\alpha)(7-2\alpha)/[2\alpha^2+(1-18\hat{\gamma}_c)\alpha+63\hat{\gamma}_c-28]$. Hereafter we assume typical cases of $\hat{\gamma}_c = 4/3$, $\hat{\gamma}_a = 5/3$ and $\alpha = 0$. Regarding ambient matter, we set $\rho_0 = 0.1 m_p \text{ cm}^{-3}$, and $R_0 = 1 \text{ kpc}$ which are typical values for elliptical galaxies (Mathews and Brighenti 2003 for review). The value of magnetic field strength in elliptical galaxies is \sim a few μG (Carilli and Taylor 2002 for review). Therefore, we fix the magnetic field strength in the shell as $B_{\text{shell}} = 10 \mu\text{G}$ where we assume the shock compression ratio being four.

Second, we show the basic treatment of photon and electron distributions in shells and lobes. We solve the following kinetic equation describing the electron energy distribution $N_e(\gamma_e, t)$ as follows:

$$\frac{\partial N_e(\gamma_e, t)}{\partial t} = \frac{\partial}{\partial \gamma_e} [\dot{\gamma}_{\text{cool}}(\gamma_e, t) N_e(\gamma_e, t)] + Q_e(\gamma_e, t), \quad (2)$$

where γ_e , $\dot{\gamma}_{\text{cool}}(\gamma_e, t) = -d\gamma_e/dt = \dot{\gamma}_{\text{ad}} + \dot{\gamma}_{\text{syn}} + \dot{\gamma}_{\text{IC}}$, and $Q_e(\gamma_e, t) \propto \gamma_e^{-p}$ are the Lorentz factor, the cooling rate via adiabatic expansions ($\dot{\gamma}_{\text{ad}} = \dot{R}\gamma_e/R$) and radiative losses and the injection rate of non-thermal electrons, respectively. Regarding IC scattering, we take the Klein-Nishina cross section into account and the following seed photons are included: (1) UV photons from a standard accretion disk, (2) IR photons from a dust torus, (3) synchrotron photons from the radio lobes, (4) synchrotron photons from the shell, and (5) Cosmic Microwave Background (CMB). As for (5), the energy density of CMB photons is sufficiently small in the present case, so we neglect it.

Third, we include the effect of absorption via $\gamma\gamma \rightarrow e^\pm$ interaction. Very high energy photons suffer from the $\gamma\gamma$ absorption via interaction with various soft photons (e.g., Coppi and Aharonian 1997). Here we include the $\gamma\gamma$ absorption due to both source-intrinsic and EBL photon fields. The $\gamma\gamma$ absorption opacity against the intrinsic photons ($\tau_{\gamma\gamma}$) can be calculated by summing up all of the photons from (1) the shell, (2) the radio lobes, (3) the dusty torus, and (4) the accretion disk and we multiply the $\gamma\gamma$ absorption factor of $\exp(-\tau_{\gamma\gamma})$ to the unabsorbed flux. For simplicity, we deal with the $\gamma\gamma$ absorption effect at the first order and we neglect cascading effect. With regard to the opacity for $\gamma\gamma$ interaction between EBL

and TeV photons, we adopt the model of Franceschini et al. (2008). They use the available information on extragalactic sources generating diffuse photons in the universe between far-UV and the sub-millimeter ranges and the opacity-corrected TeV blazars spectra are consistent with standard photon generation processes which lead to intrinsic photon indices steeper than $\Gamma_{\text{intrinsic}} = 1.6$ (e.g., Aharonian et al. 2006 and references therein).

The model parameters are as follows. As for radio lobes, the fractions of non-thermal electron energy and magnetic energy are defined as $\epsilon_{e,\text{lobe}}$ and $\epsilon_{B,\text{lobe}}$, respectively. The spectral index, the gyro factor, the minimum and maximum Lorentz factors of non-thermal electrons are denoted as p_{lobe} , ξ_{lobe} , $\gamma_{\text{lobe,min}}$, and $\gamma_{\text{lobe,max}}$, respectively. As for a shell, the fraction of non-thermal electron energy to the total internal energy is defined as $\epsilon_{e,\text{shell}}$. The spectral index, the gyro factor, the minimum and maximum Lorentz factors of non-thermal electrons are expressed as p_{shell} , ξ_{shell} , $\gamma_{\text{shell,min}}$, and $\gamma_{\text{shell,max}}$, respectively. Using the electron gyro factor ξ_i ($i = \text{lobe}$ or shell), the electron acceleration rate with its energy $\gamma m_e c^2$ is given by $d\gamma/dt = 3eB\dot{R}(t)^2/20\xi_i m_e c^3$. Hereafter we assume $\gamma_{\text{lobe,min}} = \gamma_{\text{shell,min}} = 1$. The observed range of the size $R(t) \equiv LS/2$ can be given by $5 \text{ pc} \leq R(t) \leq 175 \text{ pc}$ which correspond to $LS/2$ of the most compact and most extended sources in the CORALZ sample, i.e. J103719+433515 and J160246+524358 (de Vries et al. 2009). In this paper, we demonstrate one typical case of $R(t) = 5 \text{ pc}$ with $z = 0.08$. Observational constraints on L_j and UV and IR luminosities at the nucleus (L_{UV} and L_{IR}) are discussed in the next section.

3. OBSERVATIONAL CONSTRAINTS

Here we show key observational constraints which restrict the model parameters.

3.1. Nucleus luminosities: L_{UV} and L_{IR}

The luminosities L_{UV} and L_{IR} are important as the seed photons for IC scattering. In young radio sources, it is difficult to estimate them directly because they are heavily absorbed by the dusty torus (e.g., Kawakatu et al. 2009; Ostorero et al. 2010). Prior works (e.g., Snellen et al. 1999; Vink et al. 2006; Orienti et al. 2010) indicate that faint compact radio sources are generally characterized by a low level of ionization. Mack et al. (2009) observed the CORALZ sample at 250 GHz with the IRAM 30-meter telescope to search for dust presence and they indeed found dust emission in a significant fraction of the sample.

Here we estimate L_{UV} and L_{IR} by means of observations of other compact radio sources. Kunert-Bajraszewska and Labiano (2010; hereafter KL10) show that low-luminosity compact radio sources' [OIII] λ 5007 luminosity $L_{[\text{OIII}]}$ $\sim 10^{40} - 10^{43} \text{ erg s}^{-1}$. Radio luminosity of KL10 sample is comparable with CORALZ one. Hence, in the case of CORALZ sample, we derive the $L_{[\text{OIII}]}$ by assuming the relation of L_{radio} and $L_{[\text{OIII}]}$ obtained for low redshift radio galaxies (e.g., Buttiglione et al. 2011; Son et al. 2012), and we obtain $L_{[\text{OIII}]} \sim 10^{40} - 10^{43} \text{ erg s}^{-1}$. Since disk's UV emission is likely a main source for the ionization of clouds in narrow line regions, it is reasonable to suppose that $L_{\text{UV}} > L_{[\text{OIII}]}$ although it is not very clear what the

re-emitting fraction is. Here we examine the case of $L_{UV} = 6 \times 10^{42}, 6 \times 10^{43}, 6 \times 10^{44} \text{ erg s}^{-1}$. Regarding the torus luminosity, Calderone et al. (2012) explore the fraction of torus re-emission of absorbed accretion disc radiation for about 4000 radio-quiet AGNs and they found that the torus reprocesses $\sim 1/3 - 1/2$ of the accretion disk luminosity. Based on their work, we assume $L_{IR} = L_{UV}/2$. The IR and UV photon energy densities at $R(t)$ are given by $U_{IR}(t) = L_{IR}/4\pi cR(t)^2$ and $U_{UV}(t) = L_{UV}/4\pi cR(t)^2$, respectively.

We note that, in a few objects, a fraction of IR seed photons may arise from a dense cocoon of dust likely deposited by a merger event (e.g., Holt et al. 2009). We do not treat this case merely for simplicity.

3.2. Radio lobe fluxes

Optical. The CORALZ sample have been identified with bright galaxies in Automated Plate Measuring machine catalogue of the first Palomar Observatory Sky Survey and some further identifications in the 6th Sloan Digital Sky Survey are added and the CORALZ sample increases in number (de Vries et al. 2009 and references therein). Since mini lobes are smaller than their host galaxies, it is hard to measure the pure emission of mini lobes.

X-ray. No X-ray observations of the CORALZ sample have been performed so far. Although the emission mechanism has not yet been confirmed (i.e., accretion disk or radio lobes), X-ray fluxes of gigahertz-peaked spectrum (GPS) and compact steep-spectrum (CSS) sources have been measured by several authors recently (e.g., Tengstrand et al. 2009). Here we regard the measured X-ray fluxes in GPS galaxies $0.7 \times 10^{-14} \text{ erg cm}^{-2} \text{ s}^{-1} \leq \nu F_\nu \leq 5.6 \times 10^{-13} \text{ erg cm}^{-2} \text{ s}^{-1}$ (Guainazzi et al. 2006) as a rough upper limit of X-ray emissions from mini-radio-lobes and mini-shells.

GeV γ -ray. Prior to the launch of *Fermi*, mini-lobes were predicted to emerge as a new population of γ -ray emitter (Stawarz et al. 2008; Kino et al. 2007, 2009). With exposure time currently accumulated by *Fermi*/LAT, however, the majority of mini-lobes remain un-detected except for NGC 1275 with $\nu F_\nu \sim 4 \times 10^{-11} \text{ erg cm}^{-2} \text{ s}^{-1}$ (Abdo et al. 2009; Nagai et al. 2010; Suzuki et al. 2012; Aleksić et al. 2012) and possible detection of 4C+55.17 (McConville et al. 2011). We consider these detections as the upper limit of shell flux. Since the measured GeV- γ flux of 4C+55.17 $\sim 1 \times 10^{-11} \text{ erg cm}^{-2} \text{ s}^{-1}$ is less luminous than NGC 1275, we set it as the upper limit.

3.3. SSA turnover frequencies of radio lobes

Synchrotron self-absorption (SSA) turnover frequencies of CORALZs lobes $\nu_{ssa,lobe}$ are typically less than a few hundred MHz (de Vries et al. 2009). It should be emphasized that we can constrain $L_j \epsilon_{B,lobe}$ from the $\nu_{ssa,lobe}$. It is well known that the SSA turnover frequency is given by $\nu_{ssa,lobe} \propto B_{lobe}^{1/5} S_{\nu,lobe}^{2/5} R_{lobe}^{-4/5}$. Since $\nu_{ssa,lobe}$, $S_{\nu,lobe}$, and R_{lobe} are observationally determined, $B_{lobe} \propto (L_j \epsilon_{B,lobe})^{1/2}$ is the only parameter where $L_j \epsilon_{B,lobe} \equiv L_{poy} = 4\pi R_{lobe}^2 c/3 \times (B_{lobe}^2/8\pi) = R_{lobe}^2 c B_{lobe}^2/6$ where L_{poy} is the Poynting power of the jet. Therefore, we stress that $L_j \epsilon_{B,lobe}$ is not a free

parameter but a well constrained quantity. With typical parameters of mini-lobes, a large jet power such as $L_j \sim 6 \times 10^{47} (R_{lobe}/2 \text{ pc})^2 (\epsilon_{B,lobe}/10^{-2})^{-1} \text{ erg s}^{-1}$ is required. The requirement of large $L_j \epsilon_{B,lobe}$ for SSA model has been already pointed out by several authors (Fanti et al. 1995; Stawarz et al. 2008).

4. RESULTS

The mini-shell parameters can be well constrained, since the forward shocks considered here resembles those in the well-studied supernovae remnants (SNRs). Following prior work constraining on SNRs parameters (e.g., Koyama et al. 1995; Ellison et al. 2001), here we set $\epsilon_{e,shell} = 0.05$, $p_{shell} = 2$, and $\xi_{e,shell} = 10$. Within the observational constraint shown in 3.1, we demonstrate the case with $L_j = 5 \times 10^{46} \text{ ergs}^{-1}$. Shell and radio lobes' kinetic luminosity are governed by $L_j \epsilon_{e,shell}$ and $L_j \epsilon_{e,lobe}$. Therefore, smaller L_j and larger $\epsilon_{e,shell}$ and $\epsilon_{e,lobe}$ lead to much the same results.

The mini lobe parameters are determined on the basis of the observational constraints discussed in §3. The radio peak flux densities of CORALZ are about $\sim 100 - 500 \text{ mJy}$ at the peak frequency $\sim 1 \text{ GHz}$ (de Vries et al. 2009) and they provide constraints $\epsilon_{e,lobe}$. So as not to violate this constraint, here we set $\epsilon_{e,lobe} = 0.01$. We assume $p_{lobe} = 2.2$ which is suggested for relativistic shocks (e.g., Bednarz & Ostrowski 1997). A large gyrofactor $\xi_{lobe} = 10^7$ is assumed due to the lack of evidence of synchrotron emission from radio lobes at optical band (e.g., Holt et al. 2007; Fanti et al. 2011).

In Fig. 2, we show typical photon spectra from mini radio lobes and the mini shell with $L_{UV} = 2L_{IR} = 6 \times 10^{43} \text{ erg s}^{-1}$, and $\epsilon_{B,lobe} = 10^{-3}$. We also plot the sensitivities adopted from the following web-pages; the *Fermi*/LAT for 1 yr integration time (<http://www-glast.stanford.edu/>), HESS (<http://www.mpi-hd.mpg.de/hfm/HESS/>), MAGIC (<http://magic.mppmu.mpg.de/>), and CTA (<http://www.cta-observatory.org/>). The thick solid and dashed lines colored in red and black display the total photon fluxes from the mini shell and mini radio lobe, respectively. The radio flux density and the SSA turnover frequency of the mini radio lobes are consistent with CORALZs. Although the predicted GeV γ -ray flux appears below the *Fermi*/LAT sensitivity curve, the distinctive double-bump structure in the IC spectrum is found reflecting UV and IR emission bumps at the core. As already shown in I11, synchrotron emission from the mini-shell is very dim. It well explains the lack of detection of shells obtained so far. On the other hand, bright IC emission is expected in VHE range and it will be detectable by CTA. In Fig. 2, the mini shell spectrum without the EBL absorption effect is shown in the thin dotted curve. From this, we see that the EBL absorption is effective above a few 10^{26} Hz . In Fig. 3, we show the corresponding optical depth for $\gamma\gamma$ absorption $\tau_{\gamma\gamma}$ plotted versus the corresponding high energy photon frequency ν . At the frequency below $\sim 10^{26} \text{ Hz}$, the number density of target photons from radio lobes is larger than that from the shell, therefore the photons from the lobe dominate the absorption opacity. Since the contribution of the shell's synchrotron photons is sufficiently small as seed photons of IC and $\gamma\gamma$ absorption, we neglect them to save computational

cost.

In Fig. 4, we present predicted spectra with smaller $L_{UV} = 2L_{IR} = 6 \times 10^{42} \text{ erg s}^{-1}$, and $\epsilon_{B,lobe} = 10^{-3}, 10^{-4}, 10^{-5}$. Here, $\epsilon_{B,lobe}$ has been carefully chosen not to exceed the observed radio lobe luminosities, i.e., $\sim (1-5) \times 10^{-15} \text{ erg s}^{-1} \text{ cm}^{-2}$ at $\sim 1 \text{ GHz}$. If L_{UV} becomes smaller, then the lobe becomes synchrotron-dominated and the synchrotron luminosity becomes larger even for the same $\epsilon_{B,lobe}$. Hence, the radio flux tends to be overproduced. We therefore search parameter values according to $\epsilon_{B,lobe} \propto L_{UV}$ so as not to overproduce the lobe radio flux. Overall features of shell spectra are similar to the case in Fig. 2, and the mini-shell spectrum is detectable by CTA. However the radio lobe IC emission is less luminous than the ones in Fig. 2 at GeV band simply because of smaller $L_{UV} = 2L_{IR}$. Seed photons for IC scattering in the mini-shell are dominated by the synchrotron photons from the lobes. In IC-dominated regime, the peak luminosity of IC emission is proportional only to the $L_j \epsilon_{e,shell}$ (see Eq. (24) in I11) and it only has a weak dependence to L_{UV} and L_{IR} . The shell luminosity at TeV range becomes slightly brighter as the synchrotron emission of the radio lobes increases. Therefore, our prediction of emission spectra does not strongly depend on the choice of L_{UV} and L_{IR} .

In Fig. 5, we further present predicted spectra with larger $L_{UV} = 2L_{IR} = 6 \times 10^{44} \text{ erg s}^{-1}$, and $\epsilon_{B,lobe} = 10^{-3}, 10^{-4}, 10^{-5}$. Overall features of shell and lobe spectra are similar to the cases in Figs. 1 and 2 the mini-shell spectrum is detectable by CTA. In this case, seed photons for IC scattering are dominated by the emission of the nucleus $L_{UV} = 2L_{IR}$. Therefore, the shell IC luminosity in the TeV band remains constant for various $\epsilon_{B,lobe}$. Interestingly the intrinsic absorption in the mini-shell produces the dip around $\sim 10^{25} \text{ Hz}$.

5. SUMMARY AND DISCUSSIONS

In the present work, we have studied non-thermal emissions from mini shells surrounding low-luminosity, mini

radio lobes. Predicted synchrotron emissions from mini-shells are very faint due to their weak magnetic field. On the other hand, IC scattering in the mini-shell is significantly effective since the energy densities of soft photons from AGN nucleus and synchrotron photons from the radio lobe are large. As a result, the IC emission from the shell overwhelms the emission from the radio lobe in VHE γ -ray range. We find that the non-thermal emission from the mini-shells can be detectable by CTA and they become a potential new class of VHE γ -ray emitters.

Among FIRST survey sources (White et al. 1997), the candidate selection of CORALZs for further VLBI confirmation had been done with the criteria of the flux density $> 100 \text{ mJy}$ at 1.4 GHz and the angular size $< 2''$ (de Vries 2009). Hence a straightforward way to increase the number of lower luminosity radio lobes is to conduct further VLBI survey with a flux density threshold lower than 100 mJy among FIRST survey sources. Then, lower luminosity lobes will be found more. Another promising way to find less luminous mini radio lobes is a deep survey with the next generation radio telescope SKA with its collecting area distributed over a large geographical area. Such deep observations will significantly increase the number of radio-dark mini-shells, new class of VHE γ -ray emitters, which can be potentially detected by CTA.

Acknowledgment

We thank the referee for suggestions to improve the paper. This work is partially supported by Grant-in-Aid for Scientific Research, KAKENHI 24540240 (MK) from Japan Society for the Promotion of Science (JSPS) and by Research Activity start-up 2284007 (NK) from the Ministry of Education, Culture, Sports, Science, and Technology (MEXT). Part of this work was done with the contribution of the Italian Ministry of Foreign Affairs and Research for the collaboration project between Italy and Japan.

REFERENCES

- Abdo, A. A., Ackermann, M., Ajello, M., et al. 2009, *ApJ*, 699, 31
 Actis, M., Agnetta, G., Aharonian, F., et al. 2011, *Experimental Astronomy*, 32, 193
 Aharonian, F., Akhperjanian, A. G., Bazer-Bachi, A. R., et al. 2006, *Nature*, 440, 1018
 Aleksić, J., Alvarez, E. A., Antonelli, L. A., et al. 2012, *A&A*, 539, L2
 Bednarz, J., & Ostrowski, M. 1998, *Physical Review Letters*, 80, 3911
 Buttiglione, S., Capetti, A., Celotti, A., et al. 2011, *A&A*, 525, A28
 Calderone, G., Sbarrato, T., & Ghisellini, G. 2012, *MNRAS*, submitted (arXiv:1204.2556)
 Carilli, C. L., Perley, R. A., & Dreher, J. H. 1988, *ApJ*, 334, L73
 Carilli, C. L., & Taylor, G. B. 2002, *ARA&A*, 40, 319
 Castor, J., McCray, R., & Weaver, R. 1975, *ApJ*, 200, L107
 Coppi, B. P., & Aharonian, F. A. 1997, *ApJ*, 487, L9
 Croston, J. H., et al. 2009, *MNRAS*, 395, 1999
 Croston, J. H., Kraft, R. P., & Hardcastle, M. J. 2007, *ApJ*, 660, 191
 de Vries, N., Snellen, I. A. G., Schilizzi, R. T., Mack, K.-H., & Kaiser, C. R. 2009, *A&A*, 498, 641
 Ellison, D. C., Slane, P., & Gaensler, B. M. 2001, *ApJ*, 563, 191
 Fanti, C., Fanti, R., Dallacasa, D., et al. 1995, *A&A*, 302, 317
 Fanti, C., Fanti, R., Zanichelli, A., Dallacasa, D., & Stanghellini, C. 2011, *A&A*, 528, A110
 Franceschini, A., Rodighiero, G., & Vaccari, M. 2008, *A&A*, 487, 837
 Funk, S., & Hinton, J. 2012, *Astroparticle Phys.* in press (arXiv:1205.0832)
 Guainazzi, M., Siemiginowska, A., Stanghellini, C., et al. 2006, *A&A*, 446, 87
 Holt, J., Tadhunter, C. N., González Delgado, R. M., et al. 2007, *MNRAS*, 381, 611
 Holt, J., Tadhunter, C. N., & Morganti, R. 2009, *MNRAS*, 400, 589
 Ito, H., Kino, M., Kawakatu, N., & Yamada, S. 2011, *ApJ*, 730, 120 (I11)
 Kawakatu, N., Nagao, T., & Woo, J.-H. 2009, *ApJ*, 693, 1686
 Kino, M., Ito, H., Kawakatu, N., & Nagai, H. 2009, *MNRAS*, 395, L43
 Kino, M., Kawakatu, N., & Ito, H. 2007, *MNRAS*, 376, 1630
 Koyama, K., Petre, R., Gotthelf, E. V., et al. 1995, *Nature*, 378, 255
 Kunert-Bajraszewska, M., & Labiano, A. 2010, *MNRAS*, 408, 2279
 Lazio, J. on behalf of Science Working Group, The Square Kilometre Array Design Reference Mission: SKA Phase I, (SCI-020.010.020-DRM-002)
 Mack, K.-H., Snellen, I. A. G., Schilizzi, R. T., & de Vries, N. 2009, *Astronomische Nachrichten*, 330, 217
 Mathews, W. G., & Brighenti, F. 2003, *ARA&A*, 41, 191

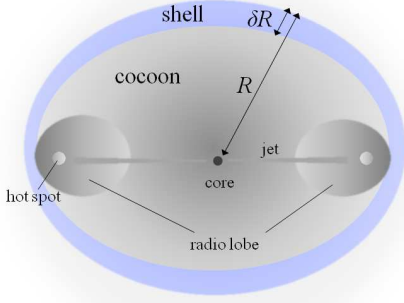


FIG. 1.— A cartoon of relativistic jets and ambient matter interaction. The kinetic energy of the jets is dissipated via shocks at the hot spots and deposited into the cocoon with its radius R and the shell with its width δR . The cocoon is inflated by its internal energy.

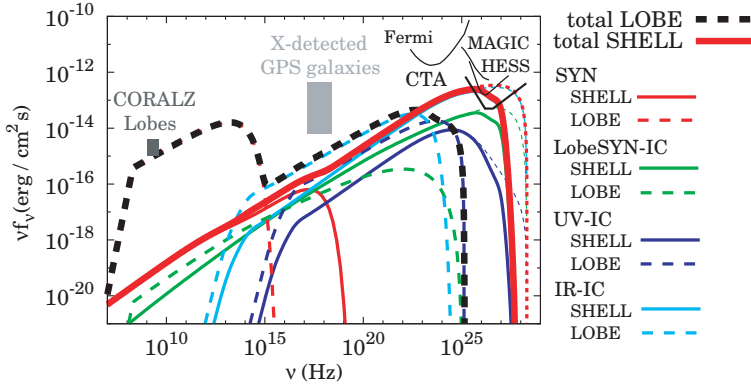


FIG. 2.— Mini-shell and radio lobe spectra (the thick red and black curves, respectively). Here, we adopt $L_{UV} = 2L_{IR} = 6 \times 10^{43} \text{ erg s}^{-1}$, and $\epsilon_{B,lobe} = 10^{-3}$. The IC components of the lobe synchrotron, UV from the accretion disk, IR from the torus, are shown in red, green, purple, blue lines, respectively. Here we plot the radio flux of typical CORALZs (de Vries et al. 2009) and also show X-ray fluxes in GPS galaxies (Guainazzi et al. 2006) as a reference.

McConville, W., Ostorero, L., Moderski, R., et al. 2011, *ApJ*, 738, 148
 Nagai, H., Suzuki, K., Asada, K., et al. 2010, *PASJ*, 62, L11
 Ostorero, L., et al. 2010, *ApJ*, 715, 1071
 Ostriker, J. P., & McKee, C. F. 1988, *Reviews of Modern Physics*, 60, 1
 Orienti, M., Dallacasa, D., & Stanghellini, C. 2010, *MNRAS*, 408, 1075
 Snellen, I. A. G., Mack, K.-H., Schilizzi, R. T., & Tschager, W. 2004, *MNRAS*, 348, 227
 Snellen, I. A. G., Schilizzi, R. T., Bremer, M. N., et al. 1999, *MNRAS*, 307, 149

Son, D., Woo, J.-H., Kim, S. C., et al. 2012, *ApJ*, 757, 140
 Stawarz, L., Ostorero, L., Begelman, M. C., Moderski, R., Kataoka, J., & Wagner, S. 2008, *ApJ*, 680, 911
 Su, M., Slatyer, T. R., & Finkbeiner, D. P. 2010, *ApJ*, 724, 1044
 Suzuki, K., Nagai, H., Kino, M., et al. 2012, *ApJ*, 746, 140
 Tengstrand, O., Guainazzi, M., Siemiginowska, A., et al. 2009, *A&A*, 501, 89
 Vink, J., Snellen, I., Mack, K.-H., & Schilizzi, R. 2006, *MNRAS*, 367, 928

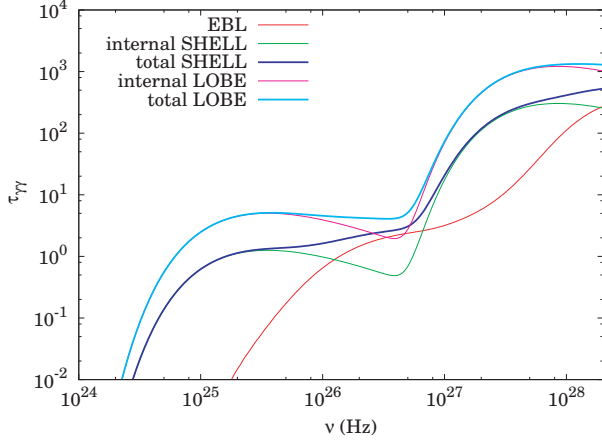


FIG. 3.— The opacity for $\gamma\gamma \rightarrow e^\pm$ corresponding to the shell spectrum in Fig. 2.

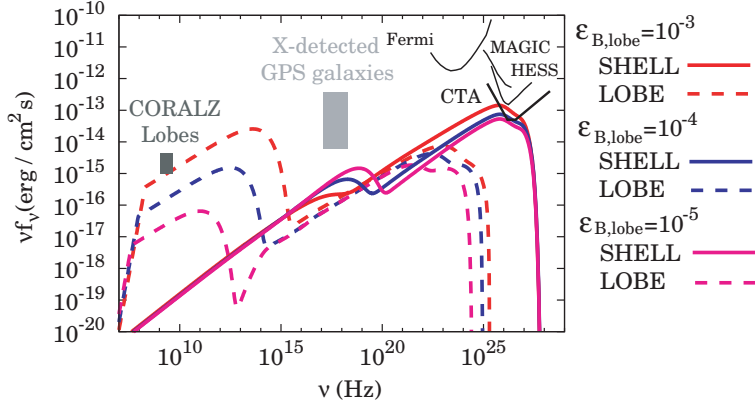


FIG. 4.— The same mini-shell and radio lobe spectra (solid and dashed curves, respectively) but with $L_{UV} = 2L_{IR} = 6 \times 10^{42} \text{ erg s}^{-1}$, and $\epsilon_{B,lobe} = 10^{-3}, 10^{-4}, 10^{-5}$. The seed photons for IC scattering in the mini-shell are dominated by the synchrotron photons of the radio lobes.

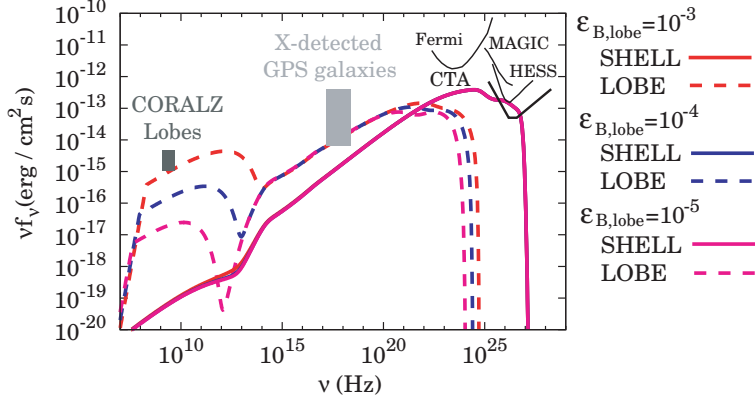


FIG. 5.— The same mini-shell and radio lobe spectra (solid and dashed curves, respectively) but with $L_{UV} = 2L_{IR} = 6 \times 10^{44} \text{ erg s}^{-1}$, and $\epsilon_{B,lobe} = 10^{-3}, 10^{-4}, 10^{-5}$. The seed photons for IC scattering in the mini-shell are dominated by the core UV and IR photons.

TABLE 1
PARAMETERS OF SHELL AND RADIO LOBES

parameters	symbols	values
jet power	L_j	$5 \times 10^{46} \text{ ergs s}^{-1}$
Distance from core to shell	R	5 pc
luminosity of IR emissions from dust-torus	L_{IR}	$3 \times (10^{44}, 10^{43}, 10^{42}) \text{ ergs s}^{-1}$
luminosity of UV emissions from accretion disk	L_{UV}	$6 \times (10^{44}, 10^{43}, 10^{42}) \text{ ergs s}^{-1}$
fraction of non-thermal electrons	$\epsilon_{\text{e,shell}}$	0.05
power-law index of injected electrons (shell)	p_{shell}	2
gyro-factor	ξ_{shell}	10
redshift	z	0.08
B energy fraction	$\epsilon_{\text{B,lobe}}$	$10^{-3}, 10^{-4}, 10^{-5}$
fraction of non-thermal electrons	$\epsilon_{\text{e,lobe}}$	10^{-2}
power-law index of injected electrons	p_{lobe}	2.2
gyro-factor	ξ_{lobe}	10^7